J Solid State Electrochem (2011) 15:269–275
DOI 10.1007/s10008-010-1109-6

ORIGINAL PAPER

Oxygen transport properties of nanostructured $SrFe_{1-x}Mo_xO_{2.5+3/2x}$ ($0<x<0.1$) perovskites

Olga Savinskaya · Alexander P. Nemudry

Received: 3 May 2010 / Revised: 12 May 2010 / Accepted: 15 May 2010 / Published online: 1 June 2010

Abstract Doping of $SrFeO_{2.5}$ with Mo^{6+} ions is accompanied by nanostructuring with the formation of 90° domains 10–20 nm in size with brownmillerite structure, as confirmed by X-ray diffraction, high-resolution electron microscopy, and Mössbauer spectroscopy. The evolution of the microstructure of $SrFe_{1-x}Mo_xO_{2.5+3/2x}$ with temperature at low oxygen partial pressure was investigated by means of high-temperature X-ray diffraction; it was shown that nanodomain texture is stable to at least $T\sim800$ °C. Chronopotentiometry and permeability measurements demonstrate that the title compounds possess high oxygen mobility within a wide temperature range: oxygen diffusion coefficients at ambient temperatures are $D=10^{-13}$–10^{-12} cm^2/s and oxygen fluxes at 960 °C for $SrFeO_{3-z}$ ($L=1.42$ mm) and $SrFe_{0.95}Mo_{0.05}O_{3-z}$ ($L=1.5$ mm) membranes in air/He gradient reach 0.25 and 0.19 μmol/(cm^2min), respectively.

Keywords Perovskite · Oxygen mobility · Nanostructuring · Oxygen-permeable membrane

Introduction

Oxides with mixed oxygen–electronic conductivity (mixed ionic electronic conductors, MIEC) attract attention due to the possibility of using them as an oxygen-permeable membrane for separation of oxygen from air, which could be integrated into catalytic membrane reactors (CMR) for partial oxidation of hydrocarbons, as well as the electrodes for solid oxide fuel cells [1, 2]. High oxygen transport properties are exhibited by membrane materials based on strontium cobaltites and ferrites with perovskite-related structure $SrMO_{3-z}$ (M = Co, Fe) and layered perovskites La_2MO_{4+x} (M = Co, Ni, Cu). Previously, it was demonstrated that unusual fast oxygen mobility in these materials is retained down to the room temperature, which is an evidence of the low activation energy of oxygen migration in these oxides [3-11]. Evidently, elucidation of the reasons of low E_a of oxygen transport in MIEC oxides is important both from the fundamental and practical points of view.

Investigations of the mechanism of unusual low-temperature oxygen transport in $SrMO_{3-z}$ (M = Co, Fe) and La_2MO_{4+x} (M = Co, Ni, Cu) were actively carried out in 1990s in the Laboratory headed by R. Schöllhorn at the Institut für Anorganische und Analytische Chemie, Technische Universität Berlin [9-14]. For brownmillerite $SrFeO_{2.5}$, disorder along the *b*-axis was detected. It was shown that the disorder is related to the high density of stacking faults, the concentration of which increased drastically in the intermediate products of electrochemical oxidation [11]. It was assumed that the extended defects (stacking faults, domain, and antiphase boundaries) could represent diffusion pathways with reduced activation energy for oxygen ionic transport [9-11]. The hypothesis is in agreement with the results on the electrochemical oxidation of $Ca_{1-x}Sr_xFeO_{2.5}$ oxides; the introduction of high concentrations of extended defects into $CaFeO_{2.5}$ by doping with Sr leads to a sharp increase in the reactivity of the matrix [12]. To describe the oxidation of nanostructured oxides with high diffusivity pathways, a phenomenological model of oxygen transport was developed [13, 14]. This model was used to determine the coefficients of

Dedicated to Prof. R. Schöllhorn on his 75th birthday

O. Savinskaya · A. P. Nemudry (✉)
Institute of Solid State Chemistry and Mechanochemistry,
Siberian Branch of Russian Academy of Science,
630128 Novosibirsk, Russia
e-mail: nemudry@solid.nsc.ru

the chemical diffusion of oxygen along domain boundaries in $Ca_{0.5}Sr_{0.5}FeO_{2.5}$ at ambient temperature [15].

On the other hand, it is known that extended defects (twin/domain boundaries) can be sustained at elevated temperatures (up to 850 °C) [16-18]. In this respect, it would be interesting to know to what extent the experience gained previously at low temperatures may be used for studying oxygen transport in membrane materials under the working conditions of CMR (T~700–1,000 °C).

It is known that strontium ferrite has different vacancy-ordered phases $SrFeO_{3-1/n}$ (n=1, 2, 4, 8, … ∞) [19, 20]. We showed previously that partial substitution of iron ions in strontium ferrite by highly charged Mo^{6+} cations results in the formation of single-phase (in terms of X-ray diffraction (XRD)) $SrFe_{1-x}Mo_xO_{2.5+3/2x}$ materials. On the other hand, oxygen stoichiometry with noninteger n value ($2 < n < 3$, $3-1/n=2.5+3/2x$, $0<x<0.1$) usually corresponds to the heterogeneous two-phase state. It should be noted that the samples having the composition $SrFe_{0.95}Mo_{0.05}O_{2.57}$ demonstrate an increase in oxygen conductivity [21].

The aim of the present work was a detailed investigation of the structure of $SrFe_{1-x}Mo_xO_{2.5+3/2x}$ ($0<x<0.1$) materials, as well as their oxygen transport properties at low and high temperatures (including the environments modeling the CMR working conditions).

Experimental

Synthesis of $SrFe_{1-x}Mo_xO_{2.5+3/2x}$ compounds was carried out using the standard ceramic method; appropriate mixtures of strontium carbonate and oxides were ground in an AGO-2 planetary ball mill, calcined at 900 °C for 6 h, and pressed into disks, which were then fired in air at temperatures of about 1,250 °C. At the final stage, the samples were kept in vacuum (P~1.33 Pa) for 2 h and quenched at room temperature. The synthesized materials were studied by means of XRD, energy-dispersive X-ray spectroscopy (EDX), Mössbauer spectroscopy, and high-resolution electron microscopy. The diffraction patterns of the samples were recorded with Bruker D8 Advance diffractometer (Sol-X energy-dispersive X-ray detector) with CuK_α radiation (λ=1.5418 Å). The examination of samples by means of high-resolution electron microscopy (HREM) was carried out with the JEM-2010 electron microscope (accelerating voltage 200 kV, point resolution 1.4 Å). The Mössbauer spectroscopy measurements were carried out using the conventional constant-acceleration technique at room temperature. The isomer shift data were given relative to the isomer shift of α-iron.

Electrochemical experiments were performed at room temperature in the galvanostatic mode (three-electrode cell, 1 M KOH electrolyte) with the working electrodes made of polycrystalline material pressed into Pt grids along with 1 wt.% of Teflon and 10 wt.% of acetylene black.

To study oxygen permeability, disk membranes with diameter of about 15 mm and L~1–1.5 mm were used. Oxygen permeation measurements were performed in the model membrane reactor similar to that described in [22] within the temperature range 775–960 °C. Glass rings (Schott glass AR) were used as the sealant to fix the gastight membrane onto a quartz tube. The effective geometric surface area of the membrane at the sweep side for permeation study was around 1 cm^2. The oxygen partial pressure at the membrane feed side was fixed at 21 kPa by blowing the ambient air at the flow rate of 150 ml min^{-1}. The helium sweep gas was supplied to the permeate side with a flow rate of 4–40 ml min^{-1}. Gas flow rates were controlled by RRG 33 mass flow controllers. A quadrupole mass spectrometer QMS 200 was used to monitor the composition of the sweep.

Results and discussion

X-ray diffraction patterns for the samples having the composition $SrFe_{1-x}M_xO_{2.5+3/2x}$ ($0\le x\le 0.1$) are presented in Fig. 1. According to XRD and EDX measurements, the materials are single phases. An increase in dopant concentration is accompanied by the transformation of the orthorhombic brownmillerite structure Imma into perovskite $Pm\bar{3}m$. The structural transition is accompanied by the transformation of the orthorhombic reflections $(240)_o$, $(042)_o$ and $(202)_o$, $(080)_o$ into cubic ones $(111)_c$ and $(200)_c$; a decrease in the intensity of reflections $(142)_o$, $(260)_o$, $(062)_o$ down to their complete disappearance at x=0.1 is observed (indices «c» and «o» relate to the cubic $Pm\bar{3}m$ and orthorhombic Imma structures, respectively). It should be noted that the structural transition proceeds through the formation of a specific orthorhombic structure; for the sample with x=0.05, the X-ray diffraction pattern is characterized by the presence of intensive basic reflections indexed in the cubic perovskite lattice and at the same time diffuse maxima (marked in Fig. 1 with asterisks); all the reflections still may be indexed in the orthorhombic cell with the parameters $a_o=c_o=\sqrt{2}a_c$ and $b_o=4a_c$. The structural features of this phase will be considered in detail below.

A convenient method of estimating the oxygen mobility and the character of phase transition depending on the oxygen stoichiometry in perovskites with mixed conductivity is chronopotentiometry [9, 12]. The dependencies of the potential of working electrode E on charge transfer q for $SrFe_{1-x}M_xO_{2.5+3/2x}$ samples ($0\le x\le 0.2$) are shown in Fig. 2. One can see that the shape of curves for compounds

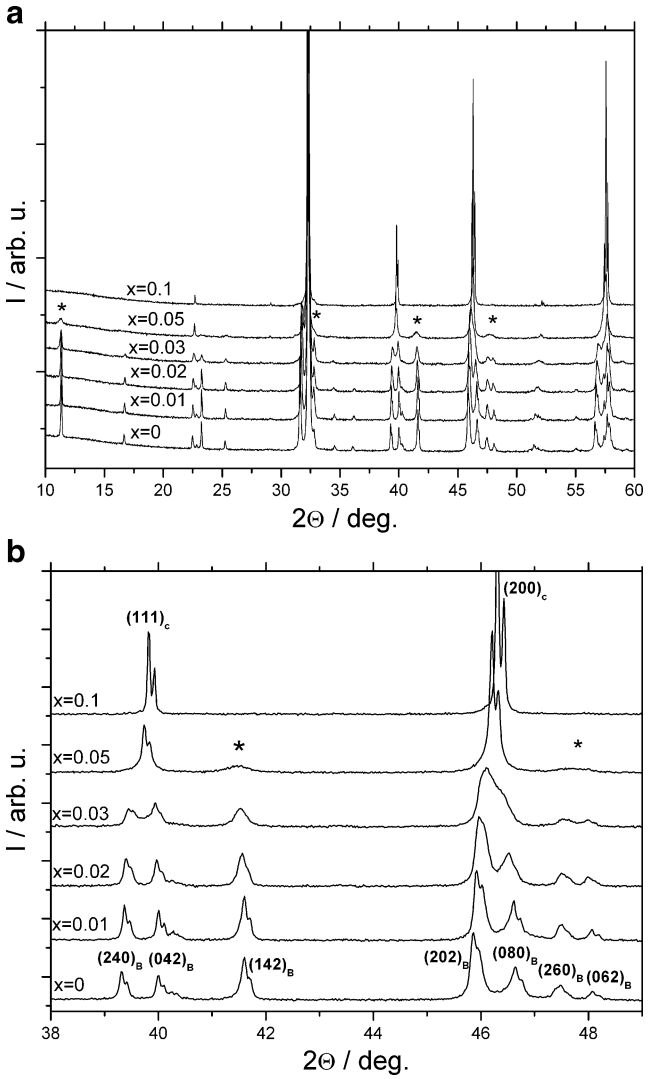

Fig. 1 **a** X-ray diffraction patterns of $SrFe_{1-x}Mo_xO_{2.5+3/2x}$ samples. **b** Sections of diffraction patters presenting the evolution of the brownmillerite reflections depending on doping level. "Superstructural" reflections marked with *asterisk*

with $x<0.1$ resembles the «$E-q$» dependencies for $SrFeO_{2.5+y}$ ($0<y<0.5$), analyzed in detail in [11], and differs only by the amount of transferred charge q (or intercalated oxygen $y=q/2$), which is related to narrowing of the region of oxygen nonstoichiometry in $SrFe_{1-x}Mo_xO_{2.5+3/2x+y}$ ($0<y<0.5-3/2x$) as a result of the incorporation of additional oxygen into the structure of strontium ferrite in order to compensate for the excess positive charge of Mo^{6+} ions. The occurrence of plateau on the curves in the region of 200–250 mV and subsequent monotonous increase in the potential up to 500–550 mV, corresponding to the reaction of the evolution of gaseous oxygen at the working electrode, provides evidence that the change of the oxygen stoichiometry from $SrFe_{1-x}Mo_xO_{2.5+3/2x}$ to $SrFe_{1-x}Mo_xO_3$ is accompanied by the formation of the intermediate products: at the first stage, as a result of the two-phase reaction and then one-phase reaction [9, 10]. It should be stressed that for the samples with $x>0.2$ the anodic polarization leads to the establishment of the potential ~500 mV at small values of charge transfer q, which is the evidence of a drop of the oxygen mobility in perovskite structure with an increase in the concentration of dopant. Estimations made on the basis of Cottrell's equation [23] provide evidence of the high oxygen mobility for $SrFe_{1-x}Mo_xO_{3-z}$ ($x<0.1$) materials; the apparent diffusion coefficients at room temperature for the title compounds are about to $D=10^{-13}$–10^{-12} cm^2/s.

Earlier, it was assumed [9-11, 15] that the fast oxygen transport at low temperatures may be related to the specific microstructure of nonstoichiometric perovskites for which the high density of extended defects (biographical ones and/or those formed during the reaction) is characteristic. For that reason, we studied the microstructure of doped $SrFe_{1-x}Mo_xO_{2.5+3/2x}$ materials.

As we have already mentioned, X-ray diffraction pattern of $SrFe_{0.95}Mo_{0.05}O_{2.58}$ compound contains broadened "superstructural" maxima (marked in Fig. 1 with asterisks) together with narrow basic perovskite reflections. The full width at half maximum (FWHM) of these broad reflections is twice as large as that of the cubic perovskite reflections. The coherence length for the sample with $x=0.05$ estimated on the basis of the FWHM of reflection (142) is about 20 nm. Similar diffraction effects were previously observed for $SrFe_{1-x}V_xO_{2.5+x}$ samples ($0<x\leq0.1$). Partial substitution of iron ions for vanadium with an increase in x also resulted in a decrease in orthorhombic distortions of the brownmillerite structure [24]. As a result, for $x=0.05$, together with intensive basic reflections indexed in the cubic perovskite subcell, broadened superstructural low-intensity reflections appeared, depicting the presence of nanosized domains (~20–50 Å). As Nakayama et al. [24] demonstrated with the help of electron microscopy, the domains had brownmillerite structure with $d_{020}=2a_c$ and were disoriented in six $<110>_c$ directions, which resulted in the superposition of spots on electron diffraction patterns and could be interpreted as the formation of the $2a_c\times2a_c\times2a_c$ supercell.

Figure 3 shows a high-resolution electron micrograph for $SrFe_{0.95}Mo_{0.05}O_{2.58}$ and corresponding fast Fourier transforms of the assigned regions, demonstrating the formation of 90° domain texture (Fig. 2, regions 1 and 2). The domains with a size of 10–20 nm, which agrees with the estimated value obtained from the FWHM of X-ray reflections, have the orthorhombic structure with d-spacing characteristic of brownmillerite with the OTOT… sequence of octahedral (O) and tetrahedral (T) layers ($d_{020}\sim2a_c\sim7.9$ Å). Superposition of diffraction patterns from the 90° domains leads to the formation of the apparent cubic cell with the parameters $2a_c\times2a_c\times2a_c$ (Fig. 3, fast Fourier transforms 3).

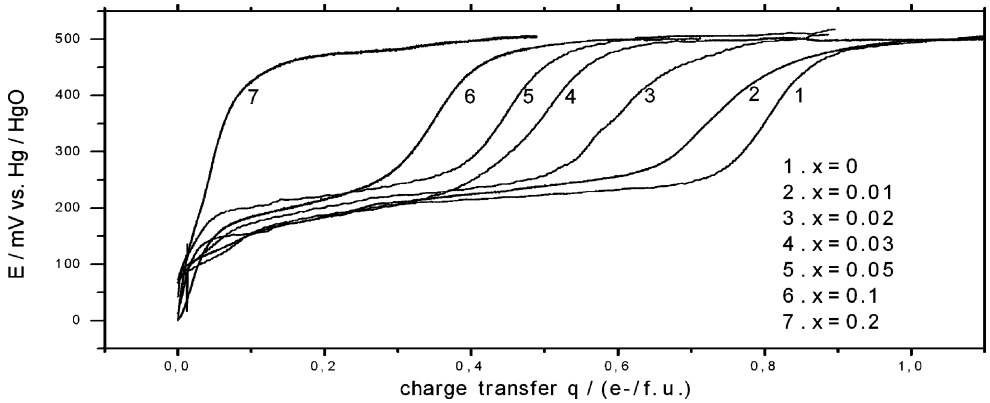

Fig. 2 Galvanostatic anodic oxidation of $SrFe_{1-x}Mo_xO_{2.5+3/2x}$ samples at room temperature in 1 M KOH electrolyte; change of potential E with charge transfer q

An increase in the molybdenum content of $SrFe_{1-x}M_xO_{2.5+3/2x}$ ($x>0.1$) suppresses the "superstructural" reflections in the X-ray diffraction patterns, which, similar to the case of $SrFe_{0.9}V_{0.1}O_{2.6}$, is likely to be connected with further disordering of tetrahedral chains as a result of a decrease in domain size down to the size of the clusters in which the oxygen vacancies are ordered at a distance several times as long as the unit cell parameter [24].

The data of Mössbauer spectroscopy are in agreement with the microscopic data and confirm the presence of domains having brownmillerite structure in $SrFe_{0.95}Mo_{0.05}O_{2.575}$ (Table 1). In the spectra of $SrFe_{1-x}M_xO_{2.5+3/2x}$ ($x\leq0.05$), two magnetically ordered sextets are distinguished; they relate to Fe^{3+} ions in the octahedral and tetrahedral positions characteristic of the brownmillerite structure (Table 1). The components ratio provides evidence of an increase in Fe^{3+} coordination when $SrFeO_{2.5}$ is doped with Mo^{6+} ions. With an increase in the dopant concentration $x\geq0.1$, the spectra are broad asymmetric lines, which depicts the formation of different coordination polyhedrons (4 (T), 5 (P), and 6 (O)) for Fe^{3+} (mainly octahedrons, due to the compensation of the excessive positive charge of the dopant).

So the structure of doped strontium ferrites may be represented as follows. A specific feature of brownmillerites, including $SrFeO_{2.5}$, is related to the presence of R and L chains in the tetrahedral layers; they can get ordered in (0k0) planes and, on the other hand, cause the formation of stacking faults along the b-axis. In addition, the formation of twins is characteristic of orthorhombic brownmillerites along the directions $[101]_b$ and $[010]_b$ [25-28]. The reason of stacking faults and twinning may be the incorporation of dopant ions and/or excess oxygen into the brownmillerite structure; acting as dilatation centers, they may provoke nucleation of twins and be localized in the twinning plane [26]. It should be noted that the presence of defects (oxygen vacancies, interstitial oxygen anions or dopant ions) localized in the tetrahedral chain may cause its gradual transformation (for instance, L chain into R and vice versa) and the formation of antiphase boundaries [26, 27]. An increase in the dopant concentration results in a decrease in the size of domains/twins (see, e.g., Fig. 2 in [29]); in our case, this is confirmed by broadening of reflections, for example (142), vs. x (Fig. 1b) to their complete smearing in the background ($x\geq0.1$). Since the 90° domains are coupled coherently, this leads to the convergence of the structural parameters in the vicinity of interfaces. As a result, at the high density of domain boundaries, the orthorhombic distortions are eliminated, and for the sample with $x=0.05$, the brownmillerite structure with parameters $a_o/\sqrt{2}=b_o/4=c_o/\sqrt{2}$ is formed inside the domains. As stressed previously, defects (dopant ions and excess oxygen) are likely to be localized within domain boundaries [24, 30].

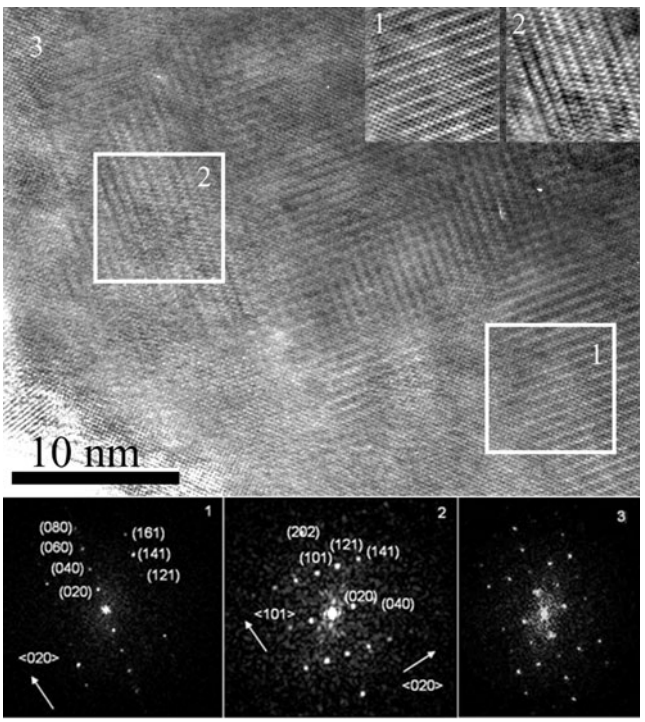

Fig. 3 High-resolution transmission electron image of $SrFe_{0.95}Mo_{0.05}O_{2.57}$ sample. Fast Fourier transforms and simulated HREM images of selected areas are shown in the *bottom* and *upper parts* of the figure, respectively

Table 1 Mössbauer parameters for $SrFe_{1-x}Mo_xO_{2.5+3/2x}$ samples

IS is the isomer shift relative to metallic α-Fe at 295 K. QS and B are the quadrupole splitting and magnetic hyperfine field, respectively. O, six-coordinated sites of Fe^{3+} cations; P, five-coordinated sites of Fe^{3+} cations; T, four-coordinated sites of Fe^{3+} cations

x in $SrFe_{1-x}Mo_xO_z$	Number	State of iron	IS (mm/s)	QS (mm/s)	B (T)	I (%)
x=0	1	Fe^{3+} (O)	0.37	−0.31	47.49	52
	2	Fe^{3+} (T)	0.16	0.29	39.92	48
x=0.05	1	Fe^{3+} (O)	0.37	−0.12	48.76	63
	2	Fe^{3+} (T)	0.18	0.18	40.97	37
x=0.1	1	Fe^{3+} (O)	0.37	−0.02	47.62	52
	2	Fe^{3+} (P)	0.25	0.01	42.75	48
x=0.2	1	Fe^{3+} (O)	0.35	−0.002	44.31	100

It should be noted that the domain and twin boundaries that may be formed in nonstoichiometric perovskites as a result of phase separation [15, 31] or ferroelastic phase transition [17, 18, 29] essentially differ from domain bulk in the distributions of electric and elastic fields [32], possess enhanced concentration of mobile defects [33], and are elastically softer with respect to the bulk, which can be the reasons of a substantial decrease in the activation energy of ion migration along domain boundaries [34]. This can provide high diffusivity paths for oxygen transport in the case of low-temperature electrochemical redox reactions.

It is an important question to be addressed whether the nanodomains are stable at high temperatures and domain boundaries contribute to the oxygen transport through perovskite membrane under the working conditions of CMR (700–1,000 °C, low oxygen partial pressure).

Since nanodomain texture is characterized by specific diffraction phenomenon, the presence of weak broadened reflections marked in Fig. 1 with asterisks, it allows one to use high-temperature X-ray diffraction as a tool to control the microstructure and to monitor its evolution under the conditions modeling a CMR. Figure 4 shows *in situ* high-temperature X-ray diffraction data of $SrFe_{0.95}Mo_{0.05}O_{2.57}$ perovskite in dynamic vacuum (P~0.51–0.81 Pa), recorded with Bruker D8 diffractometer and a high-temperature chamber HTK-16. The data obtained provide evidence that the nanodomain texture is stable to at least T~800 °C, although some "superstructural" reflections (marked with asterisks) survive up to T=1,200 °C at low oxygen partial pressure (permeate side of the membrane). The stability of $SrFe_{0.95}Mo_{0.05}O_{2.57}$ microstructure at high temperatures is in agreement with the data obtained by Orlovskaya et al. [17]. The authors demonstrated by means of in situ high-temperature TEM studies that perovskites based on $LaCoO_3$ have a dense network of twin boundaries, existing up to the temperature of the ferroelastic phase transitions at T~850 °C and get restored reversibly with a decrease in temperature (twin memory effect [18]).

Figure 5 presents the dependences of oxygen fluxes on helium sweep rate for $SrFeO_{3-z}$ (a) and $SrFe_{0.95}Mo_{0.05}O_{3-z}$ (b) membranes at different temperatures. An increase in helium flow leads to a drop of the partial pressure of oxygen at permeate side and an increase in oxygen permeation fluxes through $SrFe_{1-x}Mo_xO_{3-z}$ (x=0, 0.05) dense ceramic membranes. The oxygen permeation fluxes reach 0.25 and 0.19 μmol/(cm^{2}min) for $SrFeO_{3-z}$ (L= 1.42 mm) and $SrFe_{0.95}Mo_{0.05}O_{3-z}$ (L=1.5 mm), respectively, under the following conditions: temperature, T=960 °C; oxygen partial pressures, P_1=21 kPa and P_2=0.7 kPa at the feed and permeate sides of the membranes, respectively. The obtained oxygen flux values are close to the oxygen permeability data for ferrite-based dense ceramic membranes studied previously [35-37].

Arrhenius dependencies of oxygen fluxes through massive membranes having the composition $SrFeO_{3-z}$ and

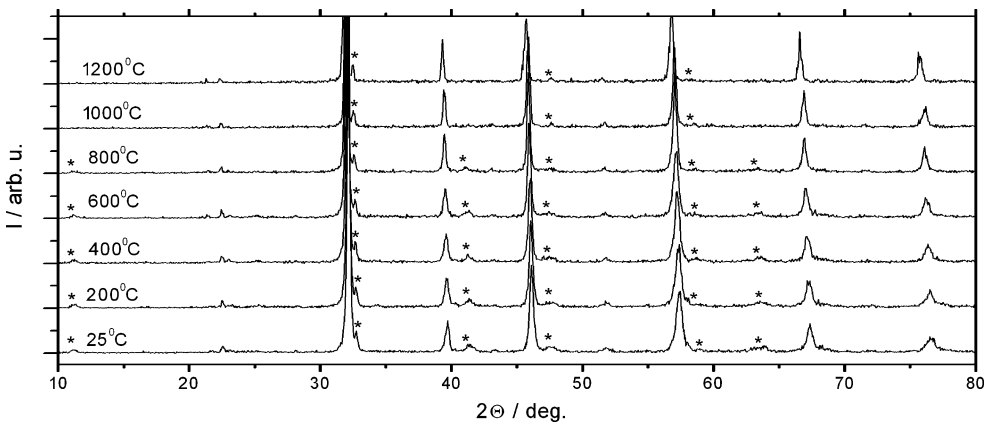

Fig. 4 In situ high-temperature X-ray diffraction data for the $SrFe_{0.95}Mo_{0.05}O_{2.57}$ sample heated in the dynamic vacuum (P~0.51–0.81 Pa). Broadened reflections related to nanodomain texture marked with *asterisks*

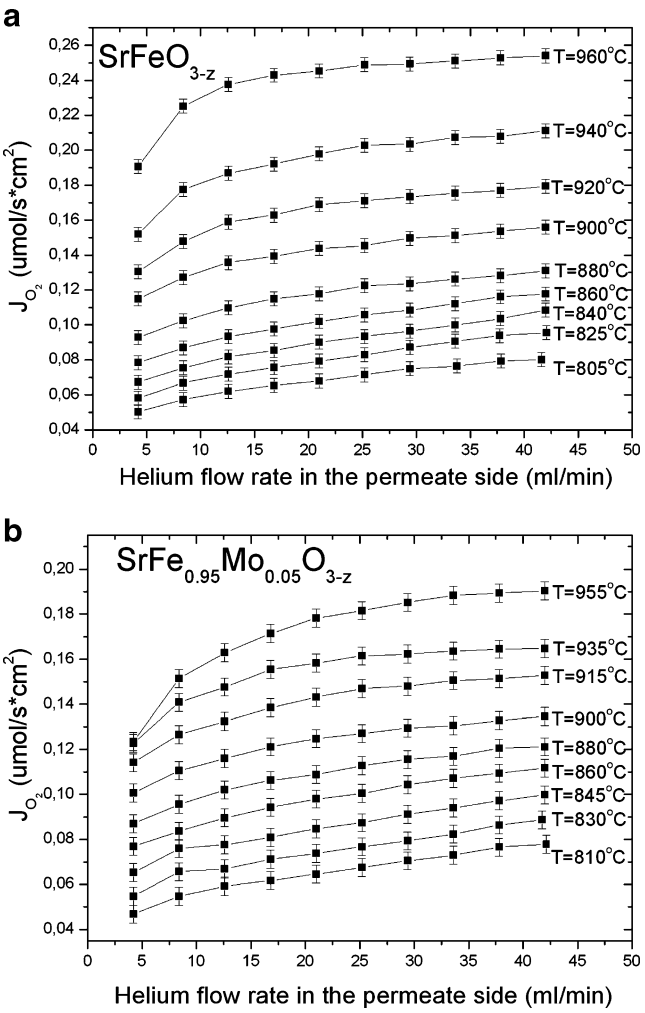

Fig. 5 Dependencies of oxygen permeation fluxes on helium flow rate at the permeate side of membranes $SrFeO_{3-z}$ (L=1.42 mm) (**a**) and $SrFe_{0.95}Mo_{0.05}O_{3-z}$ (L=1.5 mm) (**b**) at different temperatures. Condition: air flow rate in the feed side is 150 ml/min, L=1.5 mm

$SrFe_{0.95}Mo_{0.05}O_{3-z}$ on reciprocal temperature are shown in Fig. 6. According to the obtained data, the calculated activation energies of oxygen transport in the air/He gradient have the values of 104±10 and 86±10 kJ/mol for $SrFeO_{3-z}$ and $SrFe_{0.95}Mo_{0.05}O_{3-z}$, respectively.

Thus, doping of strontium ferrite with molybdenum results in a decrease in the activation energy of oxygen transport through the gastight membranes. According to literature data, strontium ferrite doping with aluminum [35] results in the opposite effect: activation energies of the oxygen transport in the air/He gradient increase with increasing dopant concentration; this gives the values of 130±10 kJ/mol for $SrFe_{0.7}Al_{0.3}O_{3-z}$. Partial substitution of strontium cations in the *A*-sublattice of strontium ferrite causes even a more substantial increase in the activation energy of oxygen transport; for instance, activation energies for the system $La_xSr_{1-x}FeO_{3-z}$ (x=0.6, 0.7, 0.8) are 173–206 kJ/mol [36].

The reasons of the different effects of doping on the activation energies of oxygen fluxes may be related to a number of factors: depending on rate-determining steps (rds) for permeability, these factors may be different catalytic properties of cations (in the case of rds as a surface reaction), trapping effects (in the case of diffusion as rds), etc. One of these factors may be the effect of doping level on the microstructure of membranes; according to the data reported in [24] and obtained in the present work, for high concentration of dopant (x>0.1), the domain structure of membrane materials may get degenerated. So a decrease in the activation energy of oxygen flux through the membrane having the composition $SrFe_{0.95}Mo_{0.05}O_{3-z}$ is in agreement with the hypothesis of the influence of domain boundaries as high diffusivity pathways on the oxygen transport in MIEC membrane materials; however, it requires additional investigation.

Conclusion

Incorporation of highly charged Mo^{6+} ions into the brownmillerite lattice brings about the fact that the accommodation of overstoichiometric oxygen is realized not due to the formation of solid solution with random distribution of extra oxygen in the structure, or phase separation, but as a result of the formation of 90° nanodomains with ordered brownmillerite structure and high concentration of domain walls accumulating excess of oxygen ions.

The data obtained provide evidence that the nanodomain texture is stable under the conditions modeling the working ones for oxygen-permeable membranes. Doping of $SrFeO_{3-z}$ by Mo^{6+} cations (x<0.2) retains the high oxygen mobility from elevated down to room temperatures.

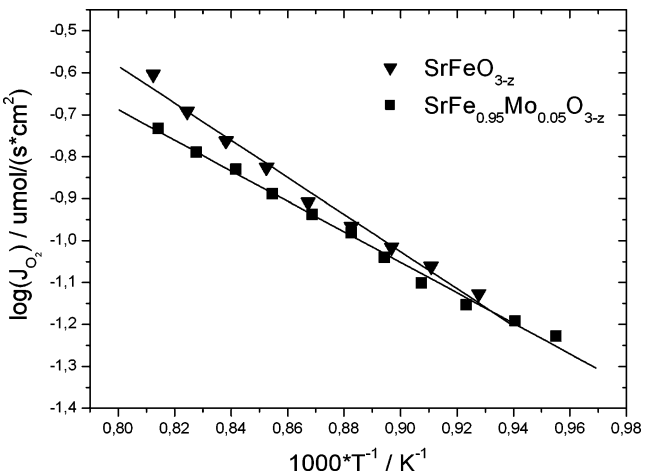

Fig. 6 Arrhenius plots of oxygen permeation fluxes through dense ceramic membranes having the composition $SrFeO_{3-z}$ and $SrFe_{0.95}Mo_{0.05}O_{3-z}$

Acknowledgements The authors are grateful to A. Ischenko and A. Nadeev (Boreskov Institute of Catalysis SB RAS, Novosibirsk, Russia) for performing HREM and high-temperature XRD measurements. The work was supported by RFBR Project No. 08-03-00738, Integration projects SB RAS (No. 82), and Presidium RAS (No. 27.54).

References

1. Bouwmeester HJM, Burgraaf AJ (1996) Dense ceramic membranes for oxygen separation. In: Burgraaf AJ, Cot L (eds) Fundamentals of inorganic membrane science and technology. Elsevier, Amsterdam, pp 435–528
2. Sunarso J, Baumann S, Serra JM, Meulenberg WA, Liu S, Lin YS, Diniz da Costa JC (2008) J Membr Sci 320:13
3. Wattiax A, Park JC, Grenier JC, Pouchard M (1990) CR Acad Sci Ser 2 310:1047
4. Wattiaux A, Fournes, Demourgues LA, Bernaben N, Grenier JC, Pouchard M (1991) Solid State Commun 77:489
5. Grenier JC, Wattiax A, Doumerc JP, Dordor P, Fournes L, Chaminade JP, Pouchard M (1992) J Solid State Chem 96:20
6. Bezdicka P, Wattiax A, Grenier JC, Pouchard M, Hagenmuller P (1993) Z Anorg Allg Chem 619:7
7. Rudolf P, Paulus W, Schöllhorn R (1991) Adv Mater 3:438
8. Takayama-Muromachi E, Sasaki T, Matsui Y (1993) Phys C 207:97
9. Nemudry A, Rudolf P, Schöllhorn R (1996) Chem Mater 8:2232
10. Nemudry A, Rudolf P, Schöllhorn R (1998) Solid State Ionics 109:213
11. Nemudry A, Weiss M, Gainutdinov I, Boldyrev V, Schöllhorn R (1998) Chem Mater 10:2403
12. Nemudry A, Rogatchev A, Gainutdinov I, Schöllhorn R (2001) J Solid State Electrochem 5:450
13. Goldberg E, Nemudry A, Boldyrev V, Schöllhorn R (1998) Solid State Ionics 110:223
14. Goldberg E, Nemudry A, Boldyrev V, Schöllhorn R (1999) Solid State Ionics 122:17
15. Nemudry A, Goldberg E, Aguirre M, Alario-Franco MA (2002) Solid State Sci 4:677
16. Adler S, Russek S, Reimer J, Fendorf M, Stacy A, Huang Q, Santoro A, Lynn J, Baltisberger J, Werner U (1994) Solid State Ionics 68:193
17. Orlovskaya N, Nicholls A, Browning N (2003) Acta Mater 51:5063
18. Savytskii DI, Trots DM, Vasylechko LO, Tamura N, Berkowski M (2003) J Appl Crystallogr 36:1197
19. Hodges JP, Short S, Jorgensen JD, Xiong X, Dabrowski B, Mini SM, Kimball CW (2000) J Solid State Chem 151:190
20. Tsujimoto Y, Tassel C, Hayashi N, Watanabe T, Kageyama H, Yoshimura K, Takano M, Ceretti M, Ritter C, Paulus W (2007) Nature 450:1062
21. Markov AA, Leonidov IA, Patrakeev MV, Kozhevnikov VL, Savinskaya OA, Ancharova UV, Nemudry AP (2008) Solid State Ionics 179:1050
22. Elshof JE, Bouwmeester HJM, Verweij (1995) Appl Catal A Gen 130:195
23. Wen CJ, Ho C, Boukamp BA, Raistrick ID, Weppner W, Huggins RA (1981) Int Met Rev 5:253
24. Nakayama N, Takano M, Inamura S, Nakanishi N, Kosuge K (1987) J Solid State Chem 71:403
25. D'Hondt H, Abakumov AM, Hadermann J, Kalyuzhnaya AS, Rozova MG, Antipov EV, Tendeloo GV (2008) Chem Mater 20:7188
26. Krekels T, Milat O, Tendeloo GV, Amelinckx S, Babu TGN, Wright AJ, Greaves C (1993) J Solid State Chem 105:313
27. Berastegui P, Hull S, Garcia-Garcia FJ, Eriksson SG (2002) J Solid State Chem 164:119
28. Lindberg F, Svensson G, Istomin SYa, Aleshinskaya SV, Antipov EV (2004) J Solid State Chemistry 177:1592
29. Salje EKH, Hayward SA, Lee WT (2005) Acta Cryst A61:3
30. Grenier JC, Ea N, Pouchard M, Hagenmuller P (1985) J Solid State Chem 58:243
31. Alario-Franco MA, Gonzalez-Calbet JM, Vallet-Regi M (1983) J Solid State Chem 49:219
32. Novak J, Fousek J, Maryska J, Marvan M (2005) Mater Sci Eng B 120:13
33. Lee WT, Salje EKH, Bismayer U (2002) Phase Transit 76:81
34. Lee WT, Salje EKH, Bismayer U (2003) J Phys Condens Matter 15:1353
35. Kharton VV, Yaremchenko AA, Valente AA, Sobyanin VA, Belyaevd VD, Semin GL, Veniaminov SA, Tsipis EV, Shaula AL, Frade JR, Rocha J (2005) Solid State Ionics 176:781
36. Elshof JE, Bouwmeester HJM, Verweij H (1995) Solid State Ionics 81:97
37. Wiik K, Aasland S, Hansen HL, Tangen IL, Odegard R (2002) Solid State Ionics 152:675